Understanding CO_2/CH_4 separation in pristine and defective 2D MOF CuBDC nanosheets via non-equilibrium molecular dynamics

Merilent T. Kallo[1], Matthew J. Lennox[1,]*

[1]University of Bath, Claverton Down, Bath, UK.

Contents

Grand canonical Monte Carlo calculations

For all grand canonical Monte Carlo (GCMC) simulations, the DREIDING force field was used for the MOF atoms with the exemption of copper atoms, the parameters of which were taken from UFF force field.[1,2] Elementary Physical Model 2 and TraPPE was used for CO_2 and CH_4 respectively.[3,4] Lennard-Jones parameters for the GCMC calculations for CuBDC, carbon dioxide and methane can be found in Table S1, S2 and S3 respectively. Partial charges for CO_2 are listed in Table S2. Partial charges for the pristine CuBDC nanosheet are included in PDB the structure file provided. Lorentz-Berthelot mixing rules were applied. 15 Å and 14 Å cut off was used for the nanosheet structures and the bulk MOF respectively for the non-bonded interactions. For the long range electrostatic interactions the Ewald method[5] was applied for the CO_2-MOF interactions and the Wolf method[6] for the CO_2-CO_2 interactions. 10 million MC steps

were used in order to allow our system to equilibrate and receive a representative average over the ensembles. The implemented temperature was 298 K. The MOF structures were assumed to be rigid. Every simulation was repeated three times. The software used was MuSiC.[7]

Table S1. Lennard-Jones parameters for CuBDC nanosheet taken from DREIDING[1] force field (with the exemption of Cu atoms which were taken from UFF[2] force field).

Atom	σ (Å)	ε (K)
Cu	3.114	2.523
O	3.033	48.285
H	2.846	7.669
C	3.473	47.982

Table S2. Lennard-Jones parameters and partial charges for carbon dioxide taken from EPM2.[8]

Atom	σ (Å)	ε (K)	Partial charge (e)
C	2.757	28.129	+ 0.6512
O	3.033	80.507	- 0.3256

Table S3. Lennard-Jones parameters for methane taken from TraPPE.[3]

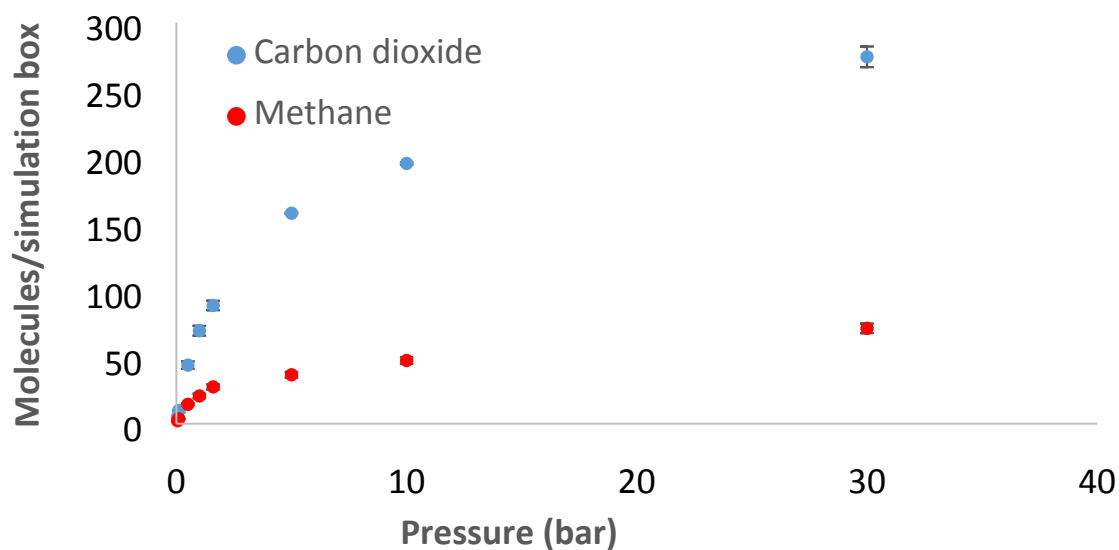| Molecule	σ (Å)	ε (K)
CH_4	3.73	148.0

Figure S1. Isotherm for the ideal CuBDC nanosheet and an equimolar CO_2/CH_4 mixture. The simulation box is as shown in Figure 1(c) of the main text.

In EF-NEMD simulations of the mixture, 90 molecules of CO_2 and 90 molecules of CH_4 were added in a simulation box containing the ideal CuBDC nanosheet structure. After an NVT equilibration, the loading of the ideal nanosheet was almost identical to the pressure point of 1.6 bar of the isotherm of Figure S1. The same pressure point was used to identify the required loading of the bulk CuBDC MOF prior to EF-NEMD simulations (i.e. the MON and bulk MOF are compared at the same external pressure,

not the same number of gas molecules in the simulation box). In Figure S2 the loading

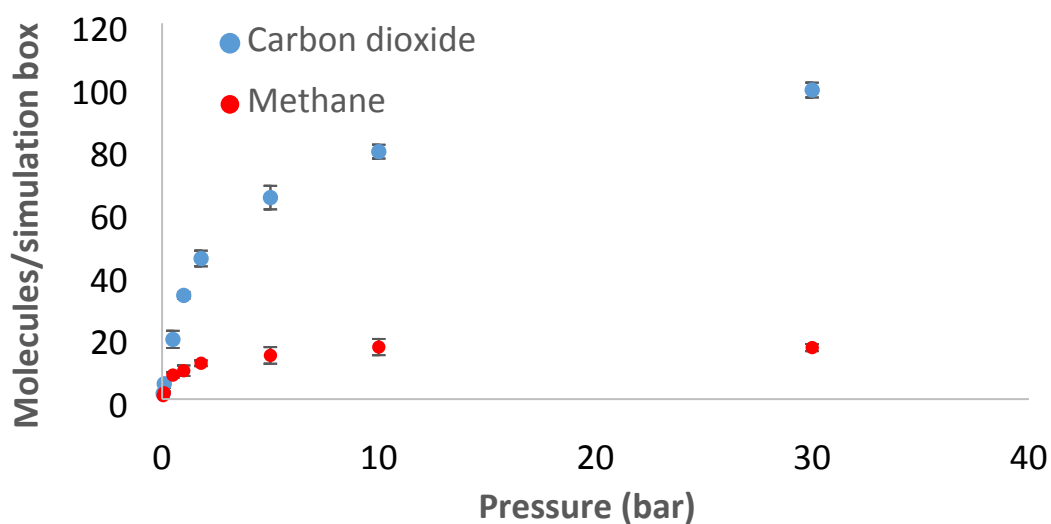of the bulk CuBDC for the simulation box used is shown.

Figure S2. Isotherm for bulk CuBDC and an equimolar CO_2/CH_4 mixture.

The isotherm for the defective structures and the equimolar mixture of CO_2/CH_4 is

presented in Figure S3. No significant differences are observed in the uptakes of the

guest molecules in the defective structures compared to the ideal nanosheet in the
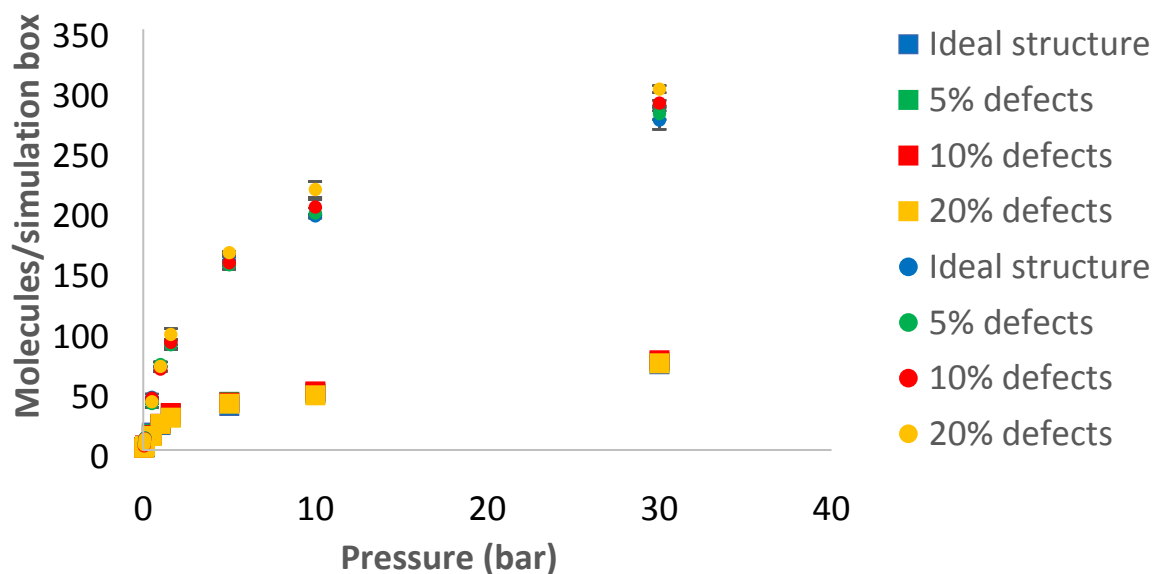
percentage range of defects studied.

Figure S3. Isotherm for ideal and defective CuBDC nanosheets and an equimolar CO_2/CH_4 mixture. Square symbols correspond to methane and circles to carbon dioxide simulated uptake. Where error bars are not shown, they are smaller than the symbols.

EF-NEMD Linear response

A linear response between the flux J_i and the pressure drop ΔP was established in every case from the analysis of external force non-equilibrium molecular dynamics (EF-NEMD) simulations. The linear relationship is confirmed in the case of an equimolar mixture in the ideal nanosheet, in the bulk CuBDC MOF and in the defective

nanosheets. The linear response is also confirmed for the case of pure components

in the ideal nanosheet. The lowest observed value of the R^2 for the linear fit was not
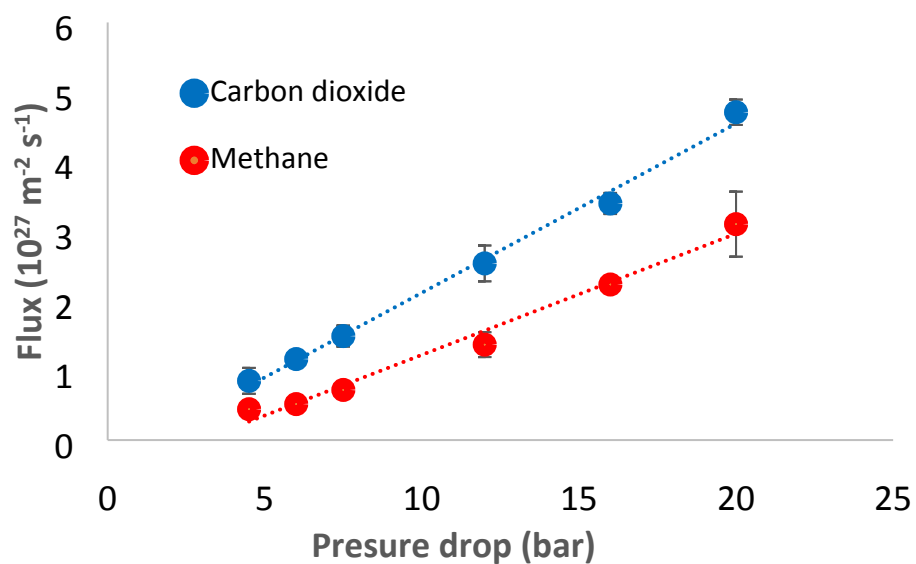
less than 0.97 in every case.

Figure S4. Linear response between the flux and the pressure drop achieved for an

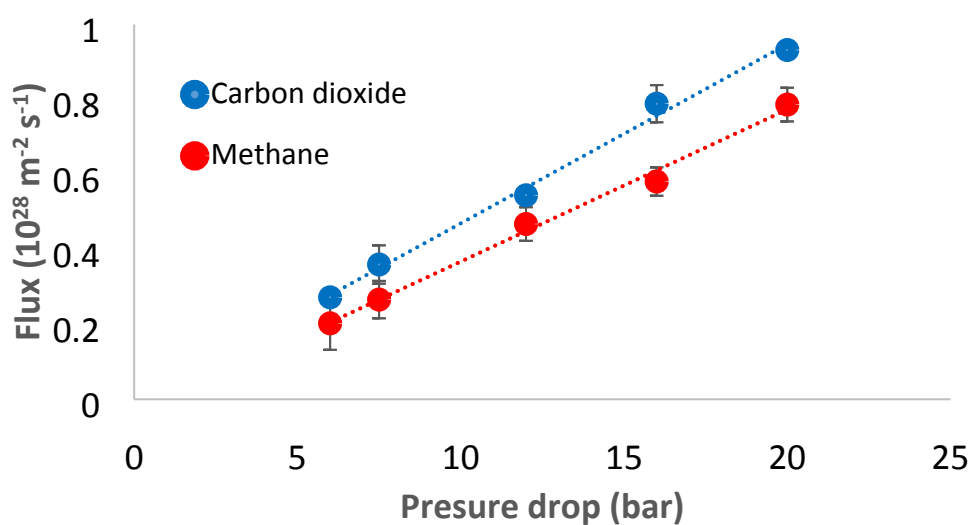equimolar CO_2/CH_4 mixture in the ideal CuBDC nanosheet.

Figure S5. Linear response between the flux and the pressure drop achieved for an equimolar CO_2/CH_4 mixture in the bulk CuBDC.
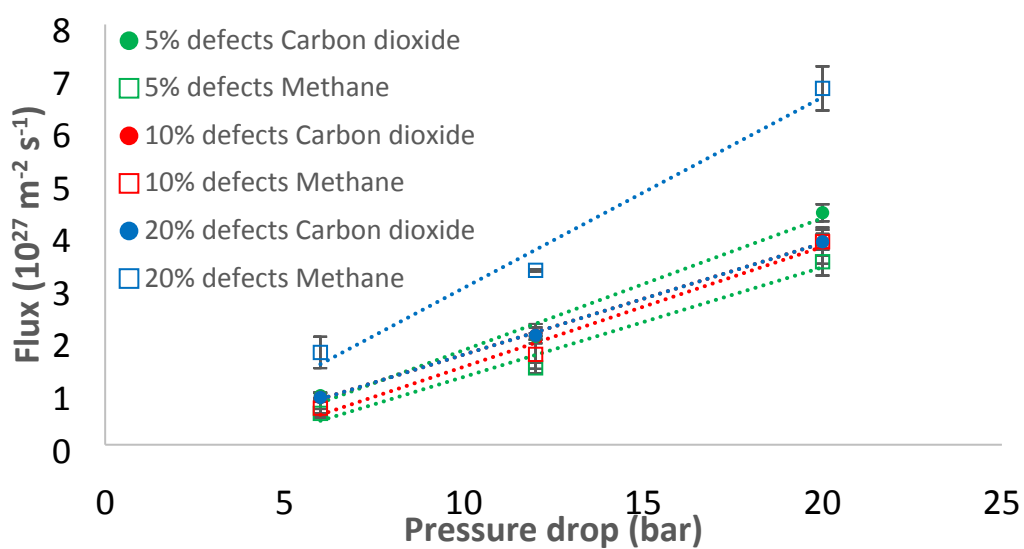

Figure S6. Linear response between the flux and the pressure drop achieved for an equimolar CO_2/CH_4 mixture in the defective nanosheet structures.
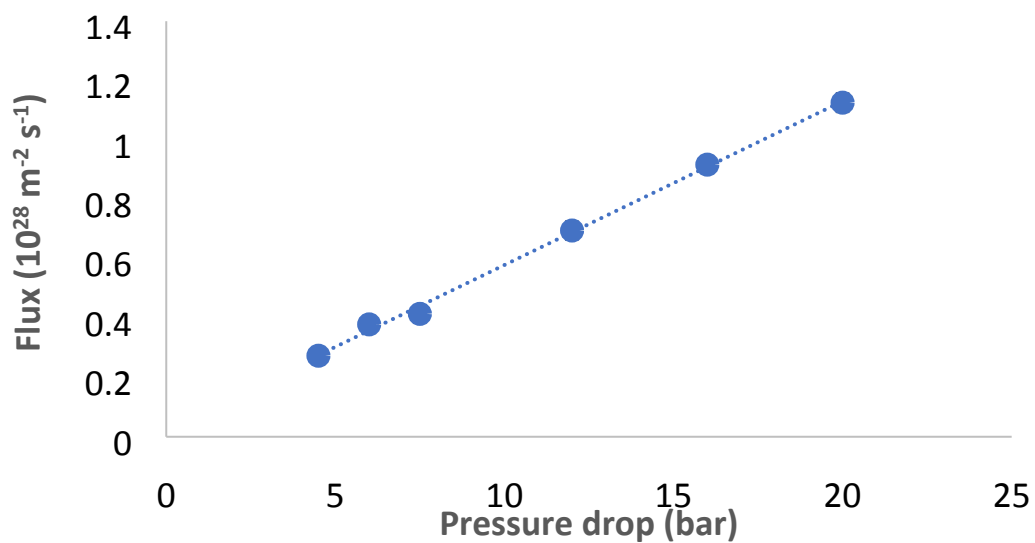
Figure S7. Linear response between the flux and the pressure drop achieved for pure
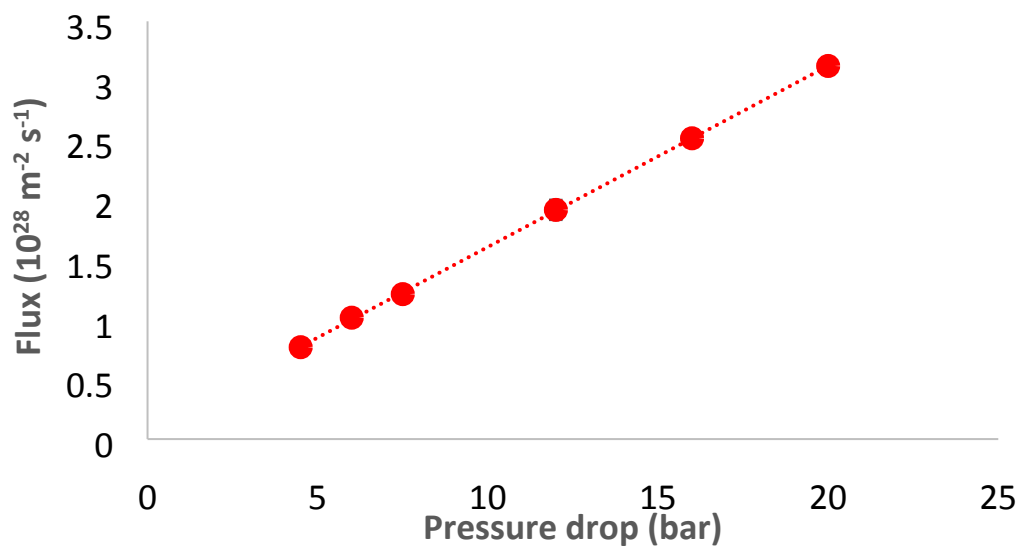
CO_2 in the ideal CuBDC nanosheet.

Figure S8. Linear response between the flux and the pressure drop achieved for pure
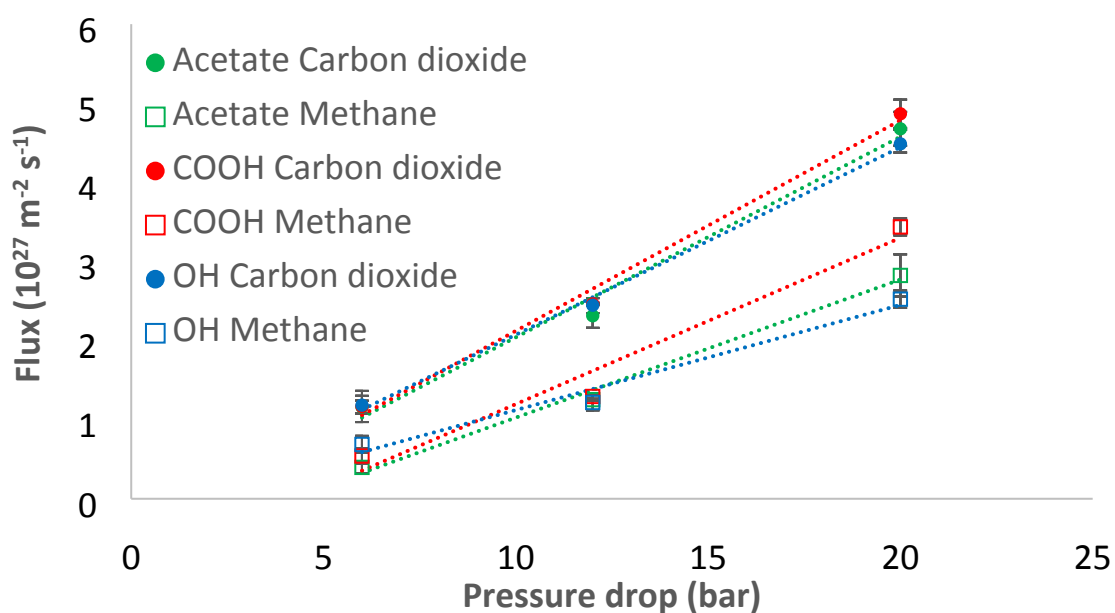
CH_4 in the ideal CuBDC nanosheet.

Figure S9. Linear response between the flux and the pressure drop achieved for an equimolar CO_2/CH_4 mixture for different surface saturations.

Density profiles

In order to evaluate whether 2 nm vacuum space on each side of the nanosheet was sufficient to eliminate finite size effects, the density profiles of CH_4 and CO_2 after the NVT pre-equilibration simulations (i.e. before the external force was switched on) were analysed (Figure S10). Three independent trajectories of 500 ns are presented. The

methane density reaches a steady value within 0.5-1 nm of the surface, indicating that
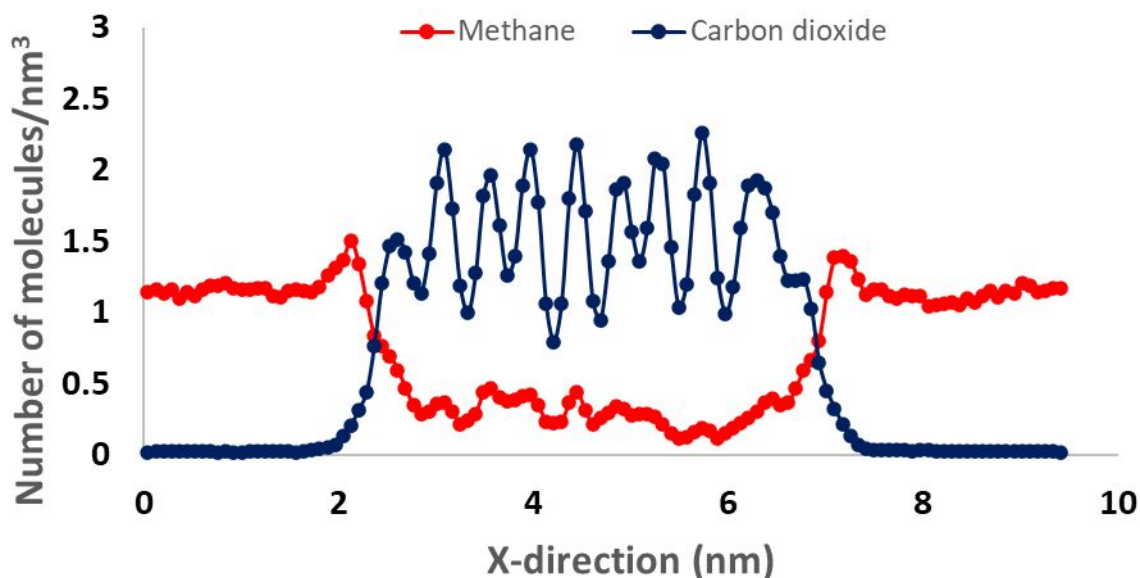
a vacuum space of 2 nm on each side is sufficient.

Figure S10. Density profiles of CH4 and CO2 in the simulation box after NVT MD equilibration, before the external force is switched on.

Density profiles from NEMD simulations are presented in Figure S11 and Figure

S12, and are averaged over 8 ns of EF-NEMD simulation run of three independent

trajectories. In Figure S11, the density profile of the MON atoms along the x-direction

is presented. MON atoms can be found only from 2.3 nm to 7.3 nm (0.5 nm thick MON)

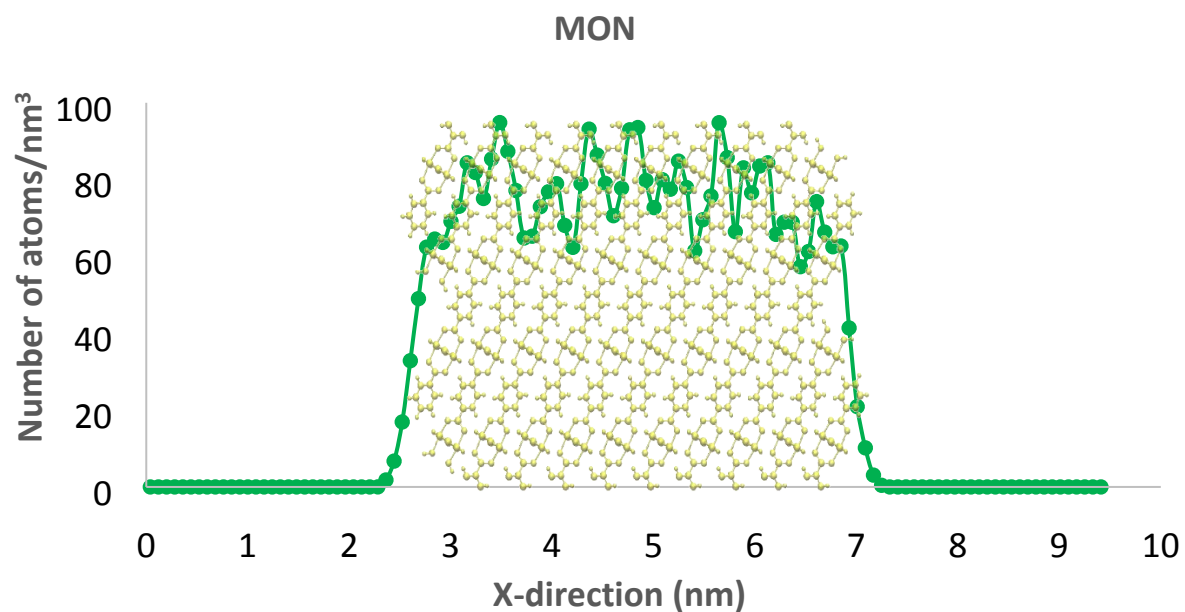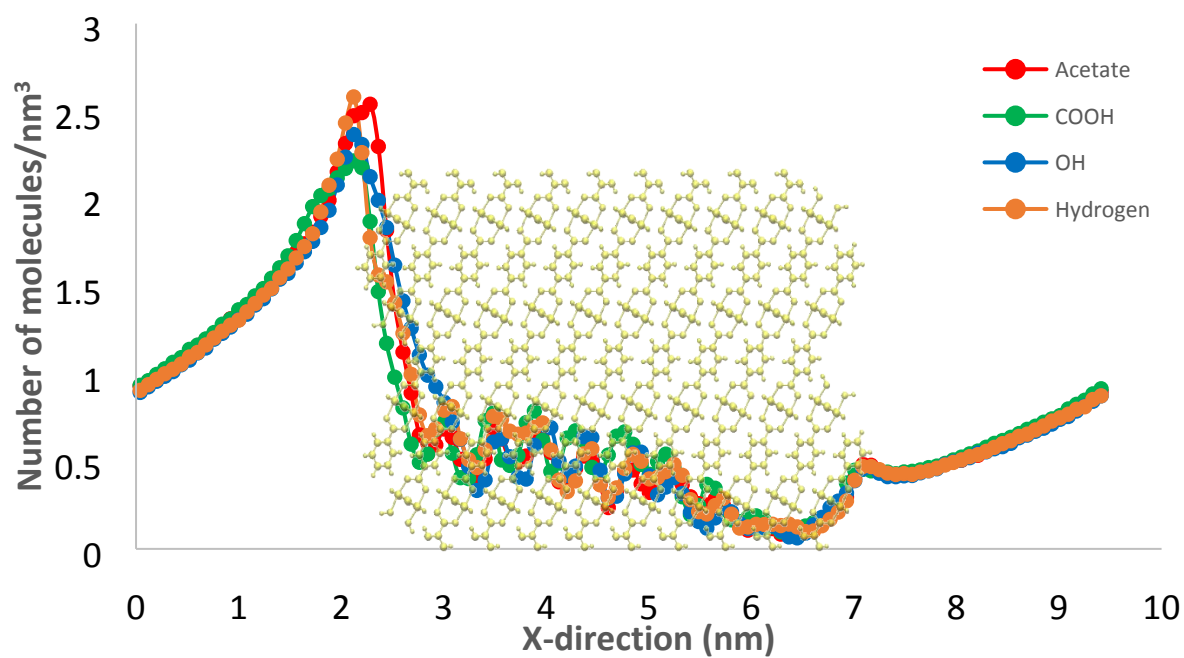as shown in Figure 1(c) in the main text.

Figure S11. Density profile of MON atoms in the simulation box. A faded image of the

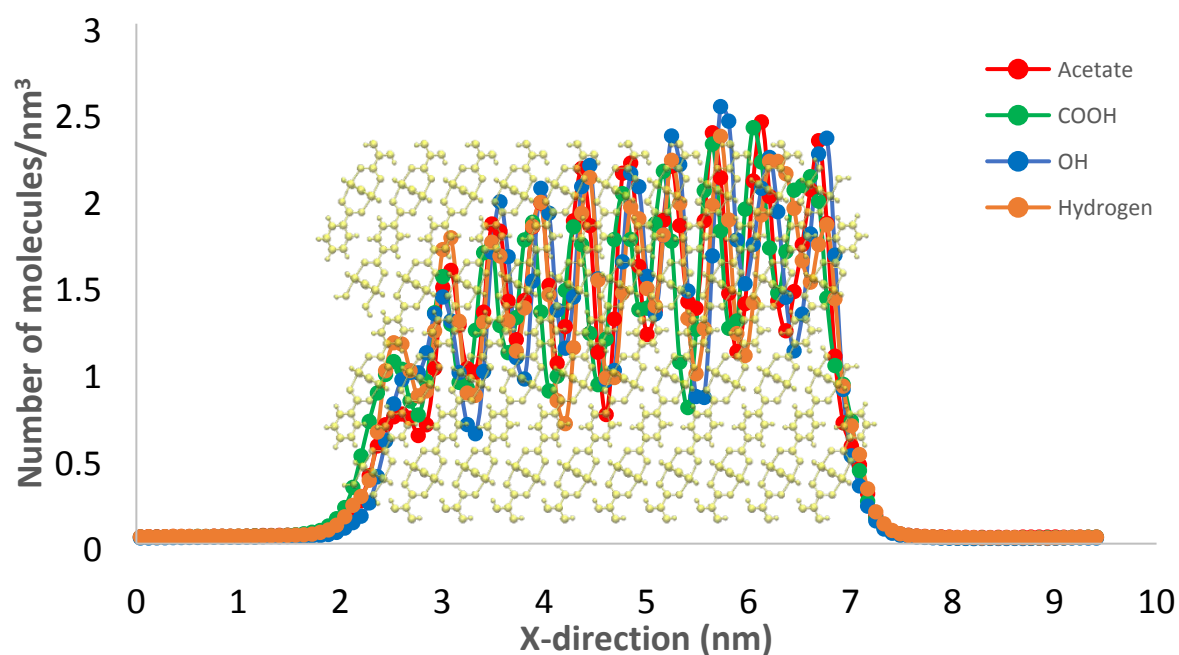nanosheet structure is added for guidance.

Figure S12. Density profile of methane (top) and carbon dioxide (bottom) for different saturation groups applied on the surface of the ideal nanosheet. The faded nanosheet corresponds to hydrogen atoms saturation.

Impact of Surface Saturation on Permeability

The selectivity and permeability are very similar for the different modulators used to saturate the surface of the nanosheet during the structure generation procedure. Acetate, carboxylic acid and hydroxyl groups are compared to hydrogen saturation.
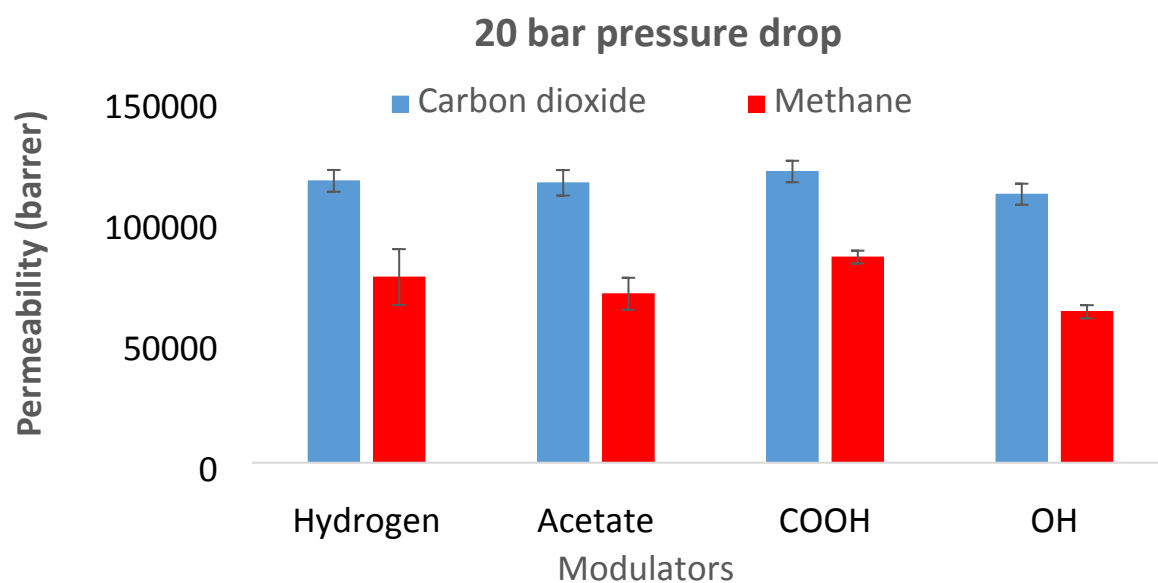
Figure S13. Permeability of methane and carbon dioxide for an equimolar mixture and
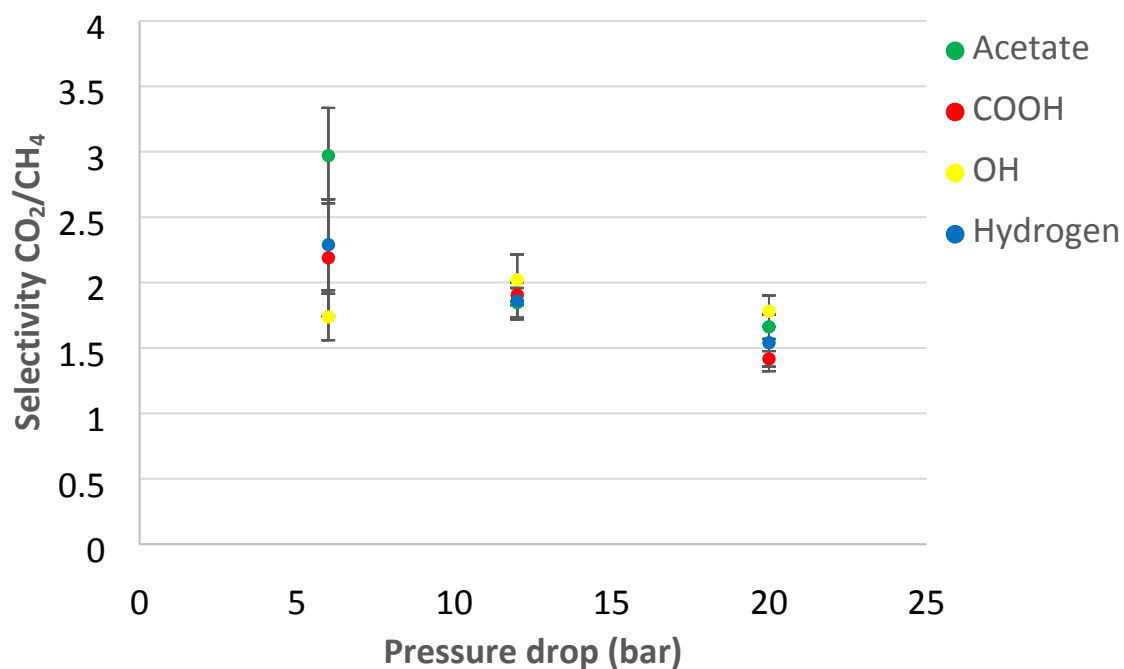
different surface saturations of the ideal nanosheet.

Figure S14. Selectivity calculated for different saturations of the ideal nanosheet surface.

Impact of Atomic Partial Charges on the Separation

EQeq charges were generated for the framework atoms of the defect-free CuBDC nanosheet.9 All other simulation parameters were the same as when Mulliken charges were used (see methodology section in EF-NEMD simulations). The effect of EQeq charges on the equimolar CO_2/CH_4 gas mixture separation was evaluated. The permeability and selectivity values calculated are within margin of error of simulations utilizing Mulliken charges. The permeability and selectivity values are shown in Figure S15 and Figure S16 respectively for 20 bar pressure drop and 298 K.
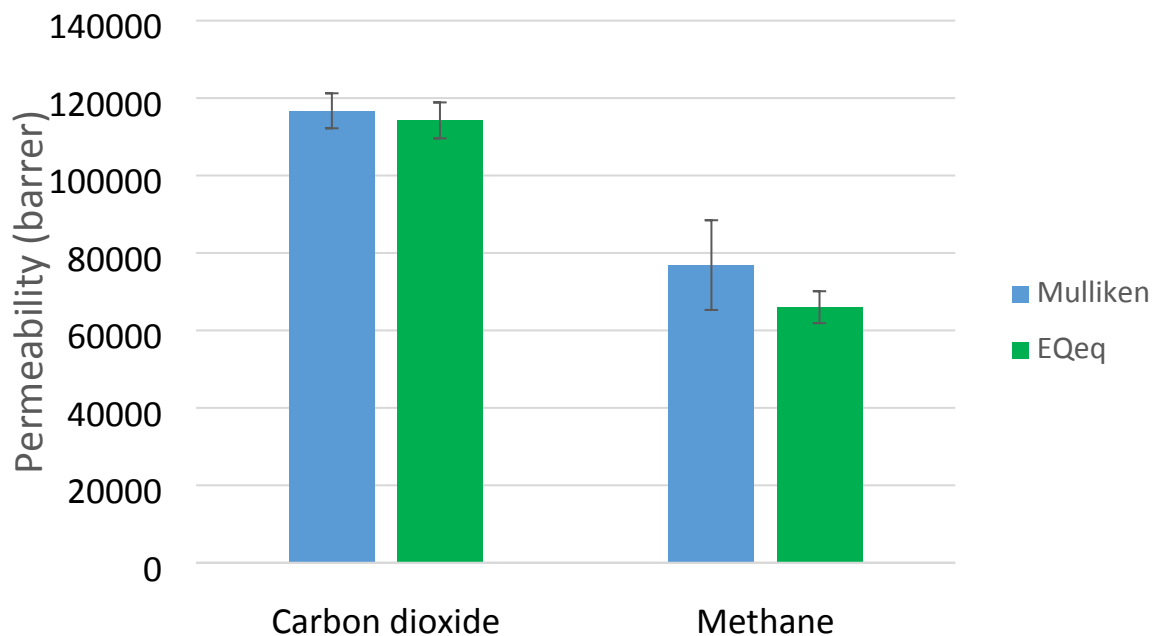
Figure S15. Permeability values for an equimolar CO_2/CH_4 gas mixture in the defect-free CuBDC nanosheet calculated with EQeq and Mulliken charges.
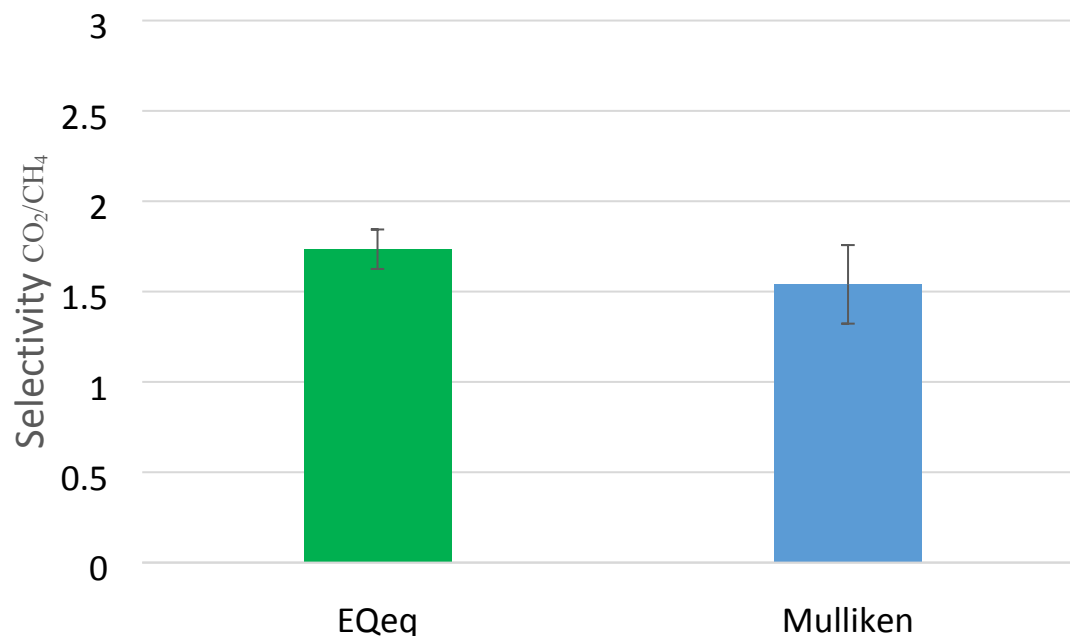

Figure S16. Selectivity of carbon dioxide over methane for an equimolar gas mixture in the defect-free CuBDC nanosheet for 20 bar pressure drop and 298 K.

Structure of non-defective CuBDC Nanosheet

The unit cell structure of a slab defect-free CuBDC nanosheet is provided as a PDB file format. Mulliken atomic partial charges are saved in the temperature factor column (column 61-66) of this file. Figure 1 (C) in the main text is a supercell of 1x2x3 unit cells.

Additional Defective Structures Studied

In order to test whether the location of defect sites influenced the calculated selectivity, one alternative structure was generated for the 5% defect concentration, and two alternative structures were generated for the 10% defect concentration. The location of the defects is shown in Figure S17. Note that there are constraints on the distributions which may be considered, as a result of the structure generation method. The defects are introduced in a small slab, for which DFT calculations are performed to obtain partial charges (to limit the number of atoms which must be considered). The supercell (nanosheet) is generated from repetitions of the smaller cell.

The selectivity of the nanosheet at a 20 bar pressure drop was calculated following the same NEMD method as described in the manuscript. It was found that the location of the defect sites does not have a qualitative impact on the selectivity or permeability of the nanosheet (Figure S18).
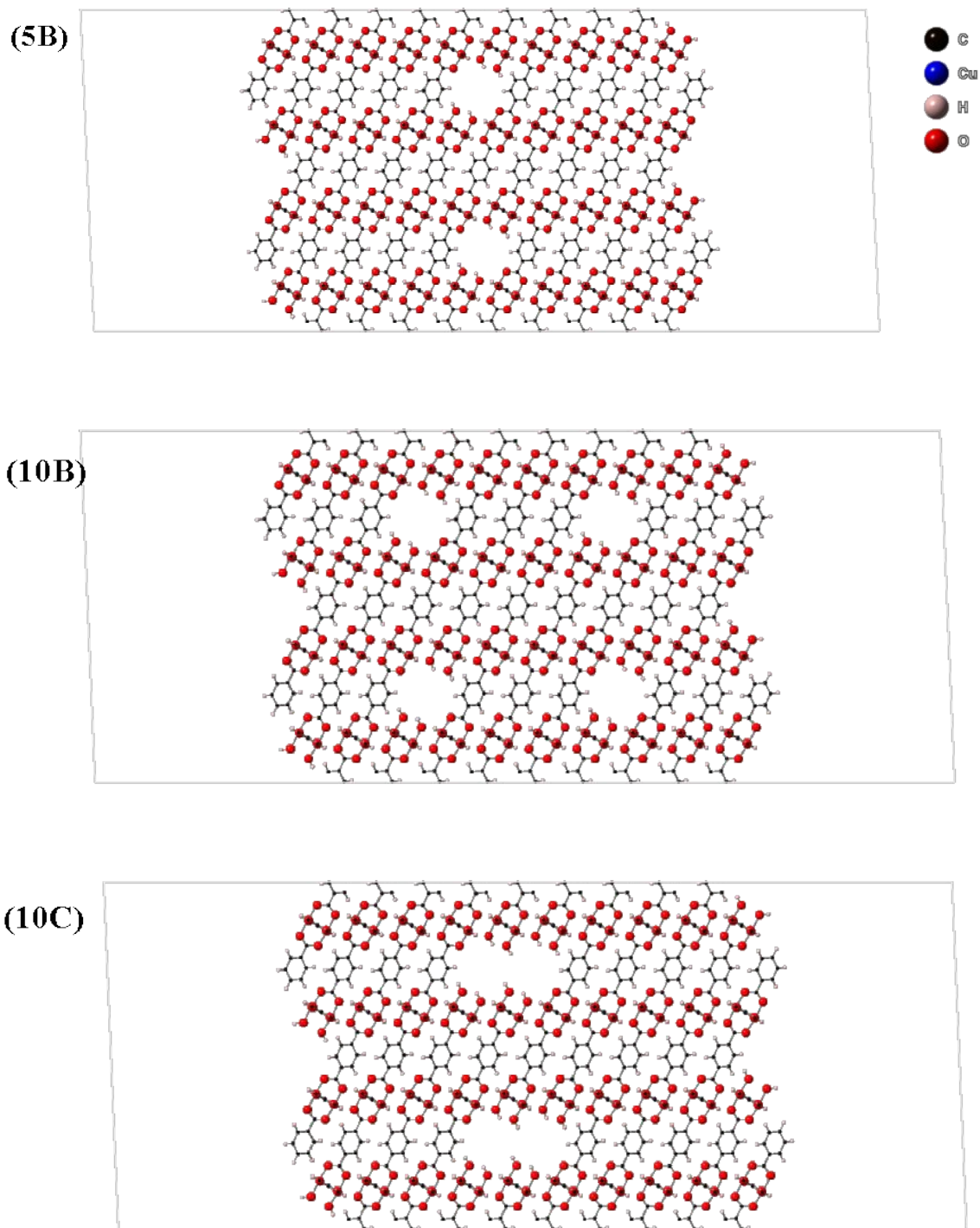
Figure S17. Structures with alternative missing linker location are shown. Top: 5B structure with 5% defects, middle: 10B structure with 10% defects, bottom: 10C structure with 10% defects.
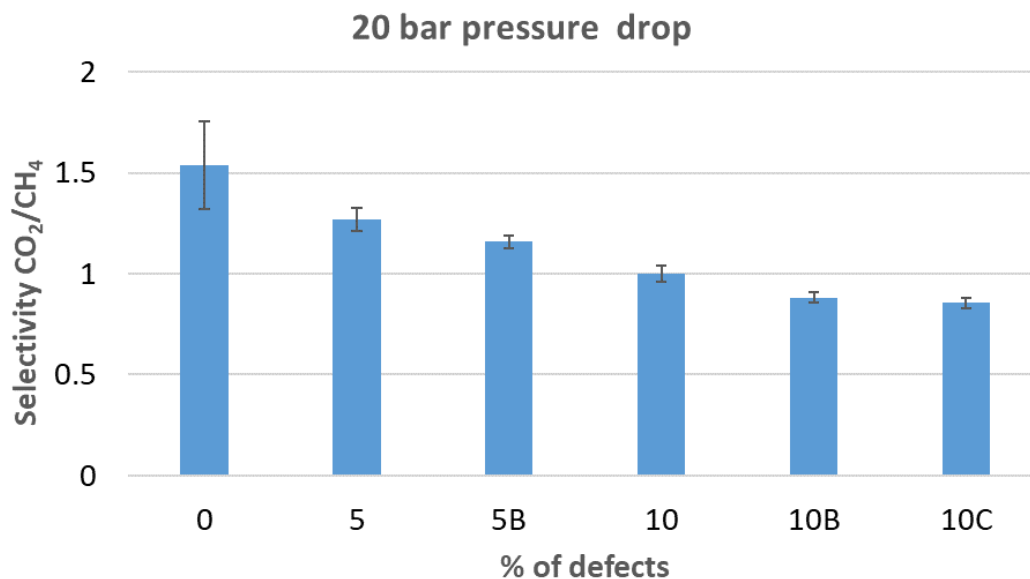
Figure S18. Calculated selectivity in the defective structures with alternative missing linker location.

References

1.   Mayo, S. L.; Olafson, B. D.; Goddard, W. A., Dreiding - a Generic Force-Field for Molecular Simulations. *J. Phys. Chem.* **1990,** *94* (26), 8897-8909.

2.   Rappe, A. K.; Casewit, C. J.; Colwell, K. S.; Goddard, W. A.; Skiff, W. M., Uff, a Full Periodic-Table Force-Field for Molecular Mechanics and Molecular-Dynamics Simulations. *J. Am. Chem. Soc.* **1992,** *114* (25), 10024-10035.

3.   Martin, M. G.; Siepmann, J. I., Transferable potentials for phase equilibria. 1. United-atom description of n-alkanes. *J. Phys. Chem. B* **1998,** *102* (14), 2569-2577.

4.   Jonathan G. Harris, K. H. Y., Carbon Dioxide's Liquid-Vapor Coexistence Curve and Critical Properties As Predicted by a Simple Molecular Model. *Phys. Chem.* **1995,** *99*.

5.   Ewald, P. P., The calculation of optical and electrostatic grid potential. *Ann. Phys.* **1921,** *64*, 253-287.

6.   Wolf, D.; Keblinski, P.; Phillpot, S. R.; Eggebrecht, J., Exact method for the simulation of Coulombic systems by spherically truncated, pairwise r–1 summation. *J. Chem. Phys.* **1999,** *110* (17), 8254-8282.

7.   Gupta, A.; Chempath, S.; Sanborn, M. J.; Clark, L. A.; Snurr, R. Q., Object-oriented programming paradigms for molecular modeling. *Mol. Simul.* **2003,** *29* (1), 29-46.

8.   Jonathan G. Harris, K. H. Y., Carbon Dioxide's Liquid-Vapor Coexistence Curve and Critical Properties As Predicted by a Simple Molecular Model. *Phys. Chem.* **1995,** *99*.

9.   Wilmer, C. E.; Kim, K. C.; Snurr, R. Q., An Extended Charge Equilibration Method. *J. Phys. Chem. Lett.* **2012,** *3* (17), 2506-11.